R. & M. No. 2653
(12,085)
A.R.C. Technical Report

MINISTRY OF SUPPLY

AERONAUTICAL RESEARCH COUNCIL
REPORTS AND MEMORANDA

Measurements of the Aerodynamic Derivatives for a Horn-Balanced Elevator

By

N. C. LAMBOURNE, B.Sc., A. CHINNECK and D. B. BETTS,
of the Aerodynamics Division, N.P.L.

LONDON: HER MAJESTY'S STATIONERY OFFICE
1953
FIVE SHILLINGS NET

Measurements of the Aerodynamic Derivatives for a Horn-Balanced Elevator

By

N. C. LAMBOURNE, B.Sc., A. CHINNECK and D. B. BETTS,
of the Aerodynamics Division, N.P.L.

Reports and Memoranda No. 2653
January, 1949

Summary.—This report gives the results of measurements by a forced oscillation method of the direct derivatives (aerodynamic stiffness and damping) for a horn-balanced elevator. The tests were made at low airspeeds on a complete wing-fuselage-tail model at 0 deg and 10 deg incidence in a wind tunnel, Some information was obtained on the effect of mean elevator angle on the derivatives when the model was at the high incidence. Measurements were also made with trailing-edge cords and transition wires in position.

The experiments suggest that none of the above factors causes a reduction in damping, but the stiffness derivative was found to be considerably influenced by the elevator angle and by the presence of trailing-edge cords and transition wires.

In general the measured values are numerically considerably less than those calculated by simple strip theory using two-dimensional vortex sheet theory results.

1. *Introduction.*—The measurements were requested in connection with a number of accidents that were attributed to flutter involving elevators. Measurements by Scruton and Raymer[1] (1943) by a decaying oscillation method had provided some knowledge of the direct aerodynamic derivatives for an elevator, but further information was required on the derivatives appropriate to an elevator with a horn balance. In addition, some indication was needed of the effects of high incidence of the tailplane, large elevator angles and the presence of trailing-edge cords. In particular, the possibility of these factors leading to a considerable reduction in damping required investigation.

2. *Range of Investigation.*—The measurements refer to the out-of-phase hinge moment (damping) and the difference between the in-phase moments in an air stream and still air (stiffness) for a range of frequencies up to 8 c.p.s. The precise form of the results is dealt with in section 5. Some measurements of the static hinge moments are included.

The main tests may be summarised under the following headings

(a) Incidence 0 deg.
(b) Incidence 10 deg (nominal).
(c) Various mean elevator angles with incidence 10 deg.
(d) Effects of ' trailing-edge cords ' and transition wires at 0-deg incidence.

(The terms ' incidence ' and ' elevator angle ' are defined by Fig. 3.)

An attempt was also made to obtain a value for the still-air aerodynamic inertia.

3. *Theory of the Method of Measurement.*—The aerodynamic hinge moment during an oscillation of the elevators may be written in the following derivative form :—

$$H = H_\eta \eta + H_{\dot\eta} \dot\eta + H_{\ddot\eta} \ddot\eta \ ,$$

where η is the elevator angle.

(52307) A

The method of determining the derivatives depended on forcing the elevator through a spring at a frequency below the resonance frequency of the system, and recording the forced motion. Fig. 4 shows diagrammatically the elevator and its associated spring system in which a sinusoidal motion, $x = x_1 \sin pt$, is given to point F. The equation of motion for the system in an airstream is of the type

$$A\ddot{\eta} + B\dot{\eta} + C\eta - Dx_1 \sin pt = H \qquad .. \quad .. \quad .. \quad (1)$$

where

A is the effective moment of inertia *in vacuo*,

B is the apparatus damping,

$C = (\sigma_1 + \sigma_2 + \Omega)r^2$, the angular stiffness (*see* Fig. 4),

and $D = \Omega r$ (*see* Fig. 4) .

The steady-state solution of equation (1) has the form

$$\eta = \eta_1 \sin (pt + \varepsilon)$$

which, when substituted in equation (1), yields the following relations :—

$$(H_\eta - p^2 H_{\ddot{\eta}}) - (C - p^2 A) = -(x_1 D/\eta_1) \cos \varepsilon \qquad .. \quad .. \quad .. \quad .. \quad (2)$$

$$pH_{\dot{\eta}} - pB = \quad (x_1 D/\eta_1) \sin \varepsilon \, . \qquad .. \quad .. \quad .. \quad .. \quad (3)$$

These are the basic equations of the method, the quantities on the right-hand sides being obtained during the measurements.

4. *Model and Apparatus.*—4.1. *General Arrangement.*—The model consisted of a complete wing-fuselage-tail unit, the major part of which had been used in the previous tests of Scruton and Raymer[1]. Fig. 5 shows the general arrangement. The wings and the forward portion of the fuselage were a $\frac{1}{6}$-th scale model of a *Blenheim* aeroplane, whilst the rear portion of the fuselage was blended into a $\frac{1}{6}$-th scale model of a *Mosquito* tail unit. The wings, the tips of which had been removed, extended to the walls of the wind tunnel (N.P.L. 7-ft No. 3), and acted as the main support for the model.

For experimental convenience, incidence was altered as follows. Steel girders rigidly attached to the ends of the wings extended downstream and were located at the walls of the tunnel in bearings in line with the elevator hinge axis. A variation of incidence thus consisted of a rotation of the model about an axis coincident with the elevator axis, the model being finally fixed by clamping the wings to the tunnel walls. Bracing wires from the rear end of the fuselage provided an additional support and eliminated flexibility of the tail unit.

4.2. *The Elevators and the Forcing System.*—The plan form and profile of half the tailplane and one elevator are shown in Fig. 6 and the principal dimensions and data are given in Table 1. The elevators were constructed from light but rigid wooden frameworks covered with stretched paper (*see* Fig. 1). They were rigidly connected by a steel shaft in line with the hinge axis and supported inside the fuselage by a ball-bearing. Each elevator was also supported by a miniature ball-bearing near its outboard end, and considerable care was taken in the alignment of these bearings so as to reduce friction.

A photograph of the elevator system is given in Fig. 2. A spring stiffness was provided by two helical springs joined by a cord that passed once round an aluminium pulley fixed to the connecting shaft. One spring was ' earthed ' to the rear of the fuselage, whilst the other was attached to a cord which could be wound up by a small electric windlass inside the fuselage. The windlass was controlled from outside the tunnel so that the mean position of the elevators was adjustable whilst the tunnel was running.

The elevators were forced through a spring connected by a cord to a second pulley on the elevator shaft. A long connecting rod transferred the motion from a reciprocating unit beneath the floor of the tunnel to the forcing spring, which, together with the connecting rod was encased in a streamlined shield extending up to the fuselage.

4.3. *The Recording System.*—The elevator motion was photographically recorded by a drum camera which received through a window in the tunnel roof an image of a light source reflected at a concave mirror attached to the elevator shaft. A spark gap fixed to the tunnel roof provided the light source, and a spark was produced each 15 deg of the forcing cycle from an induction coil operated by a commutator on the reciprocating unit. An additional segment on the commutator gave a further spark at the beginning of each cycle, which acted as a phasing datum. To prevent arcing at the segments a high-speed relay was introduced between the commutator and the induction coil. This relay introduced a time lag in the occurrence of a spark that was dependent on frequency, and for each record an appropriate phase correction was deduced from the position of the commutator segments at the instant a spark occurred. This position was observed stroboscopically by viewing the commutator in the light of a neon lamp connected in series with, and thus flashing in synchronism with, the spark gap.

The light from a second spark gap operated from a 50-c.p.s. tuning fork was reflected at a stationary mirror mounted on the tailplane, and also focussed on to the drum camera. This provided a time scale and also a datum line on the photographic records. The actinic intensities of the sparks were increased by using magnesium electrodes.

A small pea lamp placed directly behind the first spark gap provided a continuous source of light for visual observation of the elevator deflections, in which case the drum camera was replaced by a ground-glass screen.

5. *The Measurements and the Form of the Results.*—5.1. *Oscillatory Measurements.*—The elevator displacements every 15 deg of the forcing motion were obtained from the photographic records and the results for 3 cycles of motion were analysed on a ' least square error ' basis to give values of the amplitude η_1 and the phase difference ε. These values were then inserted in the right-hand side of equations (2) and (3).

The frequency of oscillation was also obtained from the record. The forcing amplitude x_1, which was adjusted for each test to give a convenient forced amplitude, was measured by a micrometer method. Its value was in the range

$$0{\cdot}19 \text{ in.} > x_1 > 0{\cdot}08 \text{ in.}$$

It was found that stretching of the connecting cords contributed to the flexibility of the elevator system, and this fact entailed the measurement of the stiffness coefficients C and D *in situ*. C was measured directly by static loading, and D was measured in terms of C by slowly rotating the forcing mechanism and observing the amplitude η_1 of the elevator in still air. D was then determined from the following relation :—

$$C\eta_1 - Dx_1 = 0 .$$

A direct determination of A, the moment of inertia, by experiments *in vacuo* could not be attempted. An indirect method of estimation was tried but it was found to be unreliable (*see* section 7), and results were accordingly based on a measurement of the total effective inertia in still air, namely

$$A - (H_{\ddot{\eta}})_{v=0} ,$$

where $-(H_{\ddot{\eta}})_{=v0}$ is the still-air aerodynamic inertia of the elevator. Thus from equation (2) it was possible to determine the following quantity

$$\bar{H}_\eta \equiv H_\eta - p^2[H_{\ddot{\eta}} - (H_{\ddot{\eta}})_{v=0}] .$$

It will be noted that $\bar{H}_\eta$ corresponds to the difference between the total in-phase moments acting during oscillations in an airstream and in still air, and the values were actually obtained from the experiments in the following form

$$\bar{H}_\eta = (x_1 D \cos \varepsilon/\eta_1)_{v=0} - (x_1 D \cos \varepsilon/\eta_1)_v .$$

The following equation is appropriate to the case of forcing in still air :—

$$C - p^2[A - (H_{\ddot{\eta}})_{v=0}] = (x_1 D/\eta_1) \cos \varepsilon .$$

From a series of experiments a plot was made of $(x_1 D/\eta_1) \cos \varepsilon$ against p^2. This showed a non-linearity as $p \to 0$, which suggested that the stiffness of the system and the effective stiffness of the forcing spring were higher in the dynamic than in the static case. It is estimated that the quoted values of both the stiffness and damping derivatives might be, on this account, some 0·5 per cent in error, which is less than the experimental scatter.

The damping derivative $H_{\dot{\eta}}$ was obtained from equation (3). A value for B, the inherent damping in the apparatus was measured by a still-air experiment before the elevator was covered, on the assumption that in this condition the aerodynamic damping of the framework would be negligible. It was found that B was very small and less than the scatter in the measurements of $H_{\dot{\eta}}$.

In equations (2) and (3) it is assumed that the aerodynamic hinge moment has the linearised form,

$$H = H_\eta \eta + H_{\dot{\eta}} \dot{\eta} + H_{\ddot{\eta}} \ddot{\eta} .$$

Non-sinusoidal motion of the elevators would certainly indicate that non-linearities, not necessarily in the aerodynamic moments, were present. However, it is likely that the non-linearities would have to be large to produce an appreciable effect at any but the lower frequencies. No serious cases of non-sinusoidal motion were obtained during the derivative measurements.

5.2. *Non-dimensional Forms.*—The results of the oscillatory measurements were finally converted to the following non-dimensional coefficients :—

$$\bar{h}_\eta = \bar{H}_\eta / \tfrac{1}{2}\rho V^2 S_\eta c_\eta$$
$$\omega_\eta h_{\dot{\eta}} = p H_{\dot{\eta}} / \tfrac{1}{2}\rho V^2 S_\eta c_\eta ,$$

where

$$\bar{h}_\eta = h_\eta - \omega_\eta^2 [h_{\ddot{\eta}} - (h_{\ddot{\eta}})_{v=0}]$$
$$h_\eta = H_\eta / \tfrac{1}{2}\rho V^2 S_\eta c_\eta$$
$$h_{\dot{\eta}} = H_{\dot{\eta}} / \tfrac{1}{2}\rho V S_\eta c_\eta^2$$
$$h_{\ddot{\eta}} = H_{\ddot{\eta}} / \tfrac{1}{2}\rho S_\eta c_\eta^3$$
$$\omega_\eta = p c_\eta / V$$

S_η area of both elevators behind hinge line

c_η mean chord of elevators behind hinge line.

5.3. *Static Hinge Moments.*—Static hinge moments were measured by observation of the equilibrium positions of the elevator in still air and in an airstream. The hinge moment H when the elevator position is η in the airstream is given by

$$H = C(\eta - \eta') - D x_1 \sin \phi ,$$

where η' is the still-air equilibrium position when ϕ, the rotation of the reciprocating gear is zero. The elevator angle at which H was measured could be varied by alteration of ϕ, and also by adjustment of the spring tension in the system.

The measured values of H were finally converted to the non-dimensional form

$$C_H = H/\tfrac{1}{2}\rho V^2 S_\eta c_\eta$$

and it will be noticed that $dC_H/d\eta$ corresponds to $h_\eta(\equiv \bar{h}_\eta)$ for $\omega = 0$.

6. *Calculation of Oscillatory Hinge Moments.*—For the purposes of calculation one semi-span tailplane and elevator were regarded as divided into strips as shown in Fig. 7. Portion ABCD was considered simply as an aerofoil with a control surface, whilst portion DCE, which included the horn, was treated as an aerofoil pitching about an axis through the elevator hinge axis.

Calculations were made for five values of the overall frequency parameter ω_η. Values of the in-phase and out-of-phase hinge moments appropriate to two-dimensional conditions were calculated for each strip from the formulae and tables given by Jones[2], the frequency parameter, chord, and flap chord for each strip being taken as those appropriate to the centre of the strip. The total hinge moment for the system was obtained by summation of the strip contributions, and the results are given in the same form as the experimental values in Table 2.

This method of calculation takes no account of the effect of finite aspect ratio, but as it is likely to be used in practice, comparisons between calculated and experimental results are valuable.

7. *Still-air Experiments and the Measurement of Aerodynamic Inertia.*—An attempt was made to estimate the inertia A of the elevator system as the sum of

A_1 (measured inertia of system with elevators uncovered),

A_2 (estimated increase due to paper covering and glue).

However, A_1 could not be determined by forcing experiments, since with the uncovered elevator the velocity damping forces were small in comparison with the frictional forces, and this led to irregular forced motions. Free oscillations were satisfactory, but the measurements of A_1 by this method were unreliable owing to possible differences between the static and dynamic stiffnesses of the system. For these reasons the derivatives were presented in a form not requiring a knowledge of A (*see* section 5).

An approximate value of the still-air aerodynamic inertia, $-(H_{ij})_{v=0}$ was obtained from the estimations of A_1 and A_2 above, in conjunction with the quantity $[A - (H_{ij})_{v=0}]$, the measured inertia of the system with elevators covered.

The value of the non-dimensional still-air aerodynamic inertia so derived was

$$-(h_{ij})_{v=0} = 0{\cdot}4\,.$$

Only single-figure accuracy appears to be justifiable, since the value is obtained as a small difference between two large quantities, $A(\equiv A_1 + A_2)$ and $[A - (H_{ij})_{v=0}]$, one of which, A, is open to suspicion.

A strip-theory calculation using two-dimensional vortex-sheet values (*see* section 6) gives

$$-(h_{ij})_{v=0} = 0{\cdot}628\,.$$

The ratio of the experimental to the theoretical value is $0{\cdot}6$, which is of the same order as the corresponding ratios referring to $\bar{h}_\eta$ and h_η (*see* section 8.1).

8. *Experimental Derivatives and Static Hinge Moments.*—The diagrams show the non-dimensional coefficients $\bar{h}_\eta$, and $\omega_\eta h_{\dot{\eta}}$ plotted against frequency parameter ω_η, and include theoretical curves for comparison. Static hinge moments are shown as the non-dimensional coefficient C_H plotted against η. Corrections for tunnel-wall interference are not attempted, but these are likely to be small since the tail unit is small in comparison with the tunnel cross-section.

The term ' incidence 10 deg nominal ' refers to the geometrical incidence in the tunnel. A simple and approximate calculation suggests that, due to downwash from the wings, the effective incidence at the tailplane would be 8 deg for this position.

During most of the tests the elevator amplitudes were within the range $4 \text{ deg} > \eta_1 > 1 \text{ deg}$.

8.1. *Incidence* 0 *deg, Mean Elevator Angle* 0 *deg, Fig.* 12.—*Amplitude Effect.*—The amplitude of the elevator motion was dependent on a number of quantities including the frequency parameter, and would have been difficult to keep constant during a series of tests. Some evidence on the effect of amplitude on the derivatives was obtained by the use of two different forcing amplitudes, one approximately twice the other, giving two sets of measurements, for various values of the frequency parameter and two wind speeds. The difference between the two sets of results were considered to be consistent with experimental scatter, and in subsequent tests any possible amplitude effect was disregarded.

Wind Speed Effect.—With 0 deg incidence and mean elevator angle 0 deg the values of $\bar{h}_\eta$ appropriate to wind speeds of 30 and 60 ft/sec differ appreciably, but the values of $\omega h_{\dot{\eta}}$ are in good agreement.

The Reynolds numbers based on the mean chord of the tailplane for the wind speeds used in the tests are as follows

V	Reynolds number
20	$0{\cdot}85 \times 10^5$
30	$1{\cdot}27$
60	$2{\cdot}54$

Comparison of Experimental with Calculated Values.—If the experimental values of $\bar{h}_\eta$ for wind speeds 30 and 60 ft/sec are meaned, the ratio of the experimental to the calculated value is approximately $0{\cdot}6$ for the static case and $0{\cdot}76$ for $\omega_\eta = 0{\cdot}4$.

A similar comparison for the damping gives an experimental/calculated ratio of approximately $0{\cdot}75$ for $\omega_\eta = 0{\cdot}4$. This is the same order as that found by Scruton and Raymer[1].

8.2. *Incidence* 10 *deg (nominal). Mean Elevator Angle* 0 *deg, Fig.* 13.—With 10 deg incidence the numerical values of $\bar{h}_\eta$ for 30 ft/sec tend to be somewhat less than those for 60 ft/sec. This is contrary to the results for 0 deg incidence. The values appropriate to 60 ft/sec for incidences 0 deg and 10 deg are in fairly good agreement.

A few measurements were made at 20 ft/sec so that the frequency parameter range could be extended. In this case there appears to be an approach towards the calculated value of $\bar{h}_\eta$ with increase of ω_η.

The damping at 10 deg incidence is slightly greater than that at 0 deg incidence.

8.3. *Incidence* 10 *deg (nominal). Various Mean Elevator Angles, Fig.* 14.—All these tests were made at 30 ft/sec, and measurements were obtained for

(a) a range of ω_η values for mean elevator angles $+ 7{\cdot}4$ deg and $+ 11{\cdot}9$ deg,

(b) a range of elevator angles for $\omega_\eta \simeq 0{\cdot}3$.

The elevator amplitudes were approximately the same throughout.

Fig. 10 showing the static hinge moment may be referred to first. Part of this diagram is reproduced on a larger scale in Fig. 11 which also illustrates the mean angles and amplitudes of the elevator during the oscillatory tests. In Fig. 11, the non-linearities in the hinge moment are treated as a change of slope in the region $\eta \doteq 3 \cdot 9$ deg. The two slopes, $dC_H/d\eta$, thus obtained have been included in Fig. 14 as points on the $\omega_\eta = 0$-axis.

The values of $\bar{h}_\eta$ (Fig. 14) show large but reasonably consistent changes with mean elevator angle. The values of ωh_η are independent of mean elevator angle for angles $-$ 8 deg to $+$ 7·4 deg, but there is an increase in the damping when the elevator angle is increased to $+$ 11·9 deg. Theoretical predictions for the same angle ranges either by the method of Schwarz and Jordan[3, 4] or by that of Jones[5] would be of interest.

8.4. *The Effect of Trailing-Edge Cords and Transition Wires.*—Cords or strips are attached in practice to the trailing edge of control surfaces to obtain desirable hinge-moment characteristics. In general the effect is to increase negatively the values of $dC_H/d\alpha$ and $dC_H/d\eta$, as shown by Batson and Warsap[6].

A few preliminary tests were made to determine the effect of cords on the static hinge moments of the model. Lengths of linen cord, 0·043 in. diameter were attached to the upper and lower surfaces of the elevators as near as possible to the trailing edges (*see* Fig. 6). The effects of these on the static hinge moments at 0 deg incidence and at 10 deg incidence are shown in Figs. 8 and 10 respectively.

A salient feature of the graphs of C_H against η for 0 deg incidence with and without trailing-edge cords, is the non-linearity. Hinge-moment curves of this type are not unusual with models in wind tunnels and improved linearity is generally effected by fixing the position of transition from laminar to turbulent flow. When the measurements already mentioned were repeated with transition wires attached to the tailplane (*see* Fig. 6) the hinge-moments curves were straightened out as shown in Fig. 9.

The results of oscillatory measurements for four conditions covering the combinations of trailing-edge cords and transition wires are shown in Fig. 15.

The mean static slopes dC_H/d_η for the range $-$ 8 deg $< \eta <$ 8 deg are included in the diagram. It will be noticed that the increments in $\bar{h}_\eta$, due to the various combinations of cords and wires, are approximately the same as the increments in the static slopes.

The addition of trailing-edge cords increases the damping. Transition wires have little or no effect on the damping when trailing-edge cords are absent, but they decrease the effect of the cords.

9. *General Conclusions.*—9.1. The tests provide no evidence that the direct damping of a horn-balanced elevator is decreased by :—

(a) High incidence.

(b) Large mean elevator angles.

(c) The presence of trailing-edge cords.

9.2. The combination of high incidence and large elevator angle may result in considerable changes in the derivative $\bar{h}_\eta$.

9.3. Trailing-edge cords and transition wires cause changes in the derivative $\bar{h}_\eta$, which are similar to the changes in the static hinge-moment slope, $dC_H/d\eta$.

10. *Suggestions for Further Research.*—Further experiments, preferably with a two-dimensional model, would be useful in order to determine in more detail the effect of elevator angle. The results with transition wires suggest that in future derivative measurements attention should be paid to the boundary-layer conditions.

TABLE 1

Model Data

Tailplane		
b_t	overall span of tailplane (tip to tip)	3·08 ft
c_t	mean chord of tailplane	0·699 ft
c_t'	mean chord of tailplane over elevator span	0·673 ft
Elevators		
b_η	sum of spans of both elevators	2·76 ft
c_η	mean chord of elevators behind hinge line	0·293 ft
S_η	sum of areas of both elevators behind hinge line	0·808 sq ft
S_H	sum of areas of both horns forward of hinge line	0·0306 sq ft
	per cent horn balance area $= 100S_H/S_\eta$	$3·78_5$

TABLE 2

Calculated Hinge Moments

ω_η	$h_\eta - \omega_\eta^2 h_{\dot\eta}$	$\bar{h}_\eta \equiv h_\eta - \omega_\eta^2[h_{\dot\eta} - (h_{\dot\eta})_{v=0}]$	$\omega_\eta h_{\dot\eta}$
0	0·9270	0·9270	0
0·159	0·7772	0·7931	0·2794
0·318	0·6885	0·7520	0·6577
0·477	0·5929	0·7358	1·0328
0·638	0·4749	0·7305	1·4031

$(h_{\dot\eta})_{v=0} = 0·6280$

REFERENCES

No.	Author	Title, etc.
1	C. Scruton and W. G. Raymer	Measurements of the Direct Elevator and Fuselage Vertical Bending Derivatives for Decaying Oscillations. (Appendix IV) R. & M. 2323. May, 1948.
2	W. P. Jones	Summary of Formulae and Notations used in Two-dimensional Derivative Theory. R. & M. 1958. August, 1941.
3	L. Schwarz	A Semi-experimental Method for Determining Unsteady Pressure Distribution. (T.B. Vol. 11 (1944) No. 5.) Translated by Sylvia W. Skan, Aero Divn., N.P.L. A.R.C. 10,387. February, 1947.
4	P. Jordan	Unsteady Aerodynamic Derivatives on the Basis of the Semi-experimental Method. 1. Tables. (F.B. 1917/1) (28.2.44). Translated by Sylvia W. Skan, Aero Divn., N.P.L. A.R.C. 10,388. February, 1947.
5	W. P. Jones	Aerofoil Oscillations at High Mean Incidences. A.R.C. 11,502. April, 1948. (To be published.)
6	A. S. Batson and J. H. Warsap	Effect on Hinge Moment of Fitting Strips near Aileron Trailing Edge, of Increasing Aileron Chord and of Extending Aileron to Wing Tip. With an Appendix on Pressures over Surface of Control Fitted with Strips. R. & M. 1936. July, 1940.

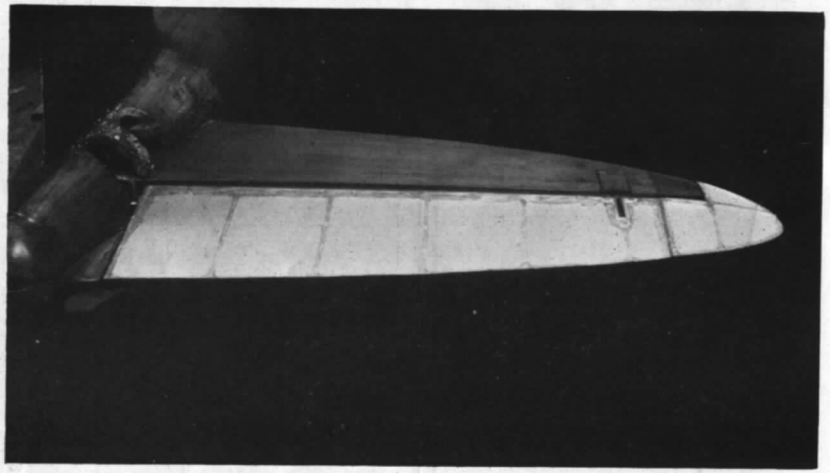

FIG. 1. General view of one elevator.

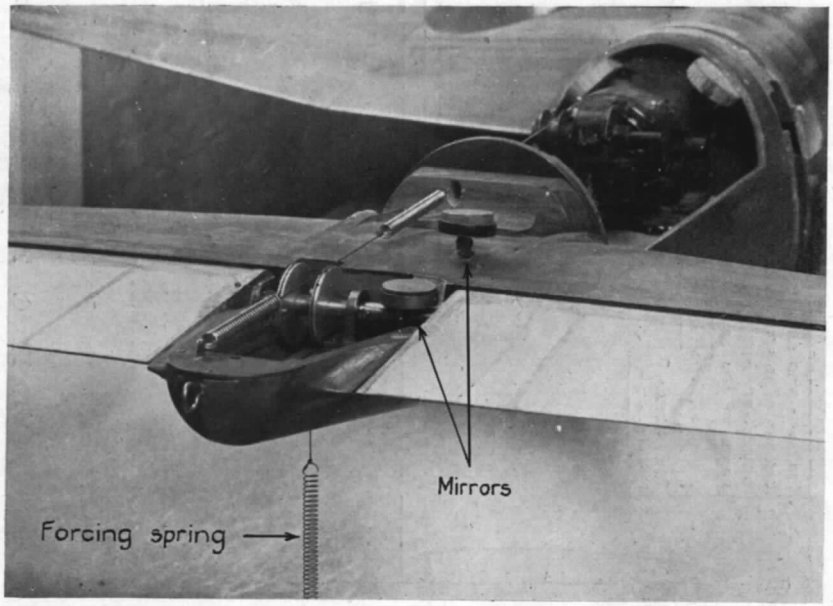

FIG. 2. The elevator spring and forcing systems.
(With fin and part of fuselage removed.)

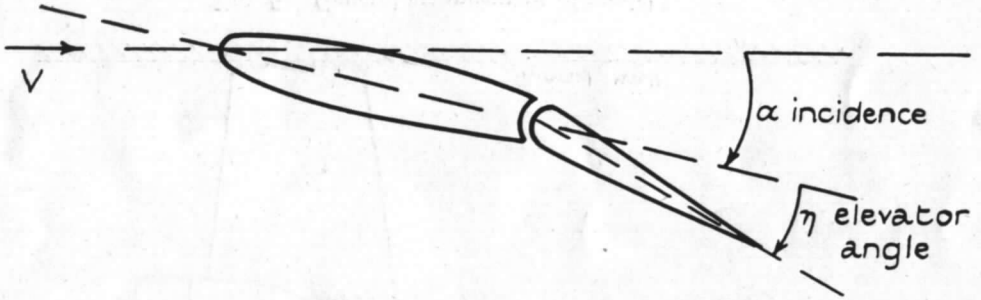

FIG. 3. Definition of incidence and elevator angle.

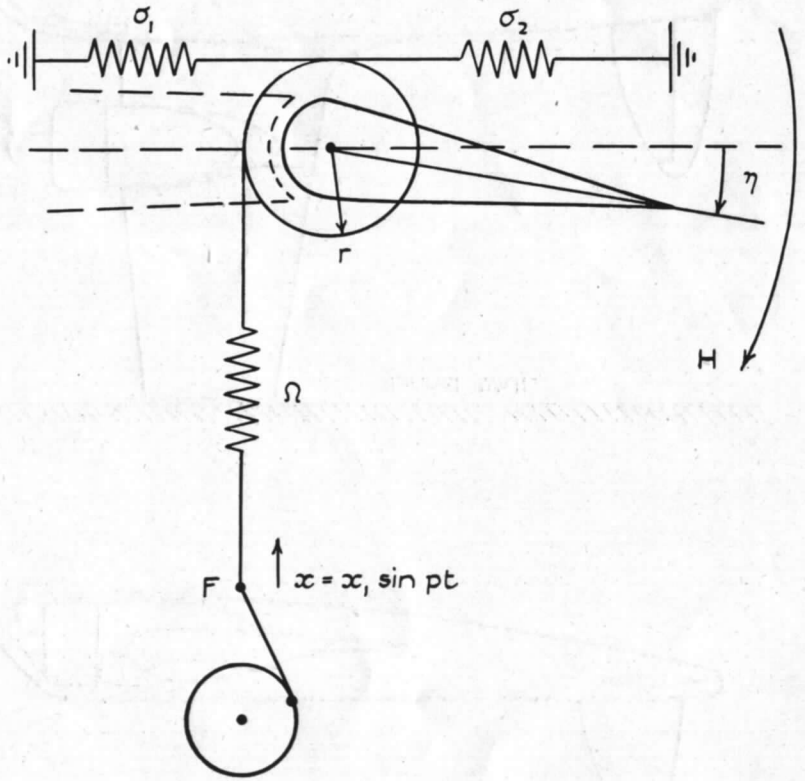

FIG. 4. Diagram of forcing system.

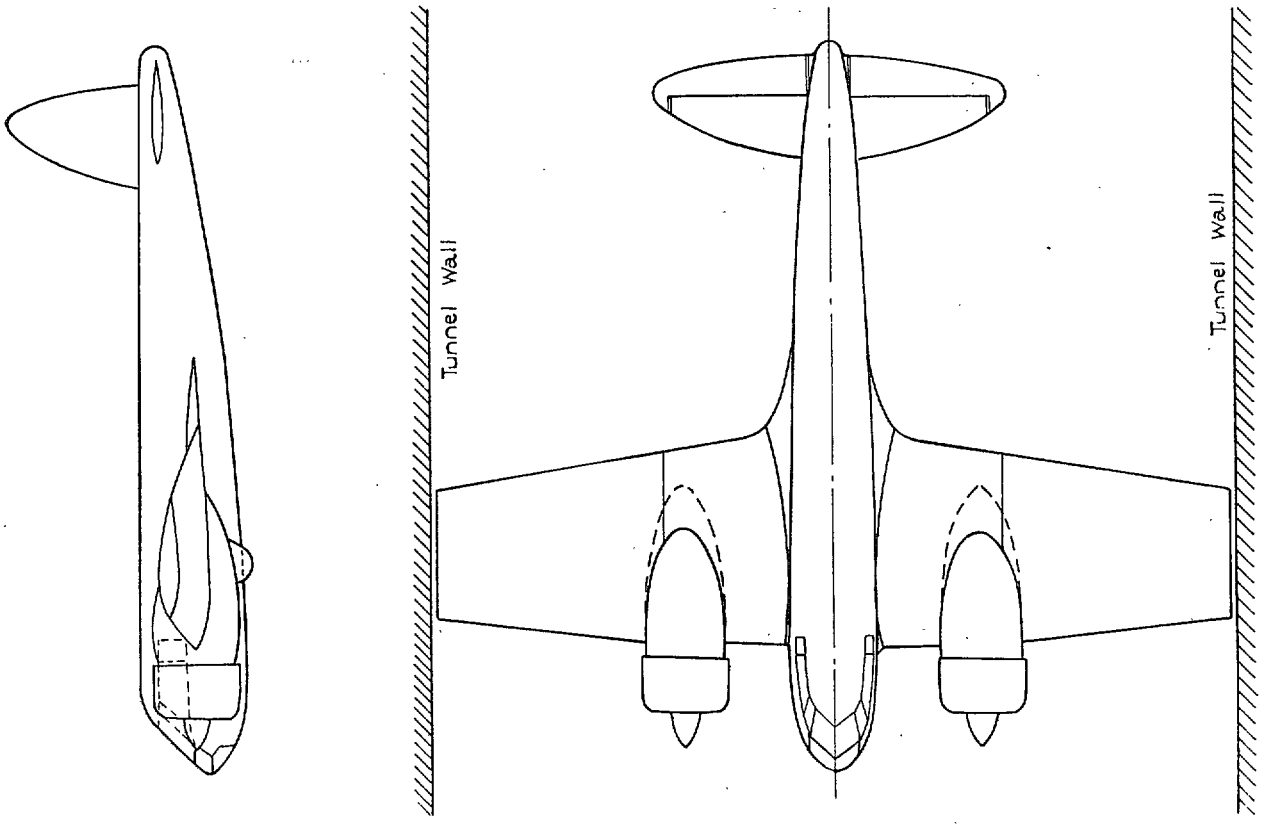

FIG. 5. General arrangement of model.

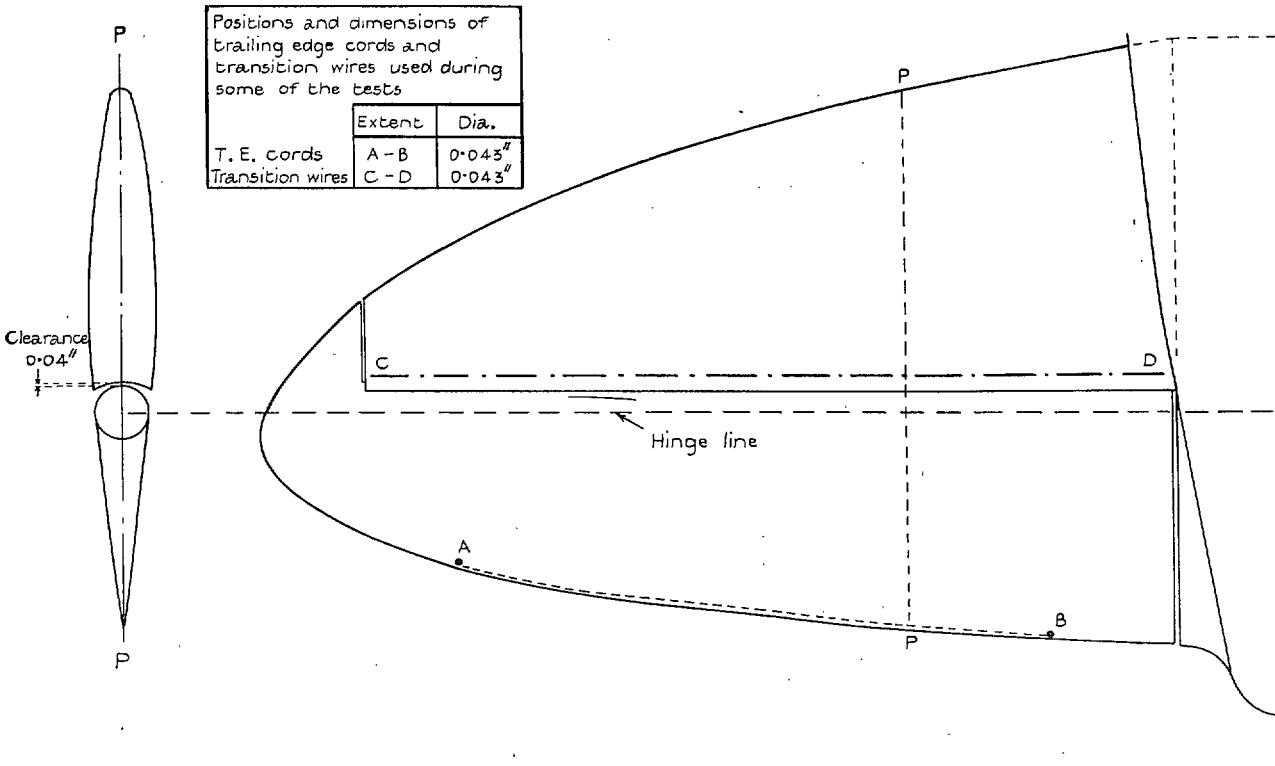

FIG. 6. Plan form and profile of tailplane and elevator.

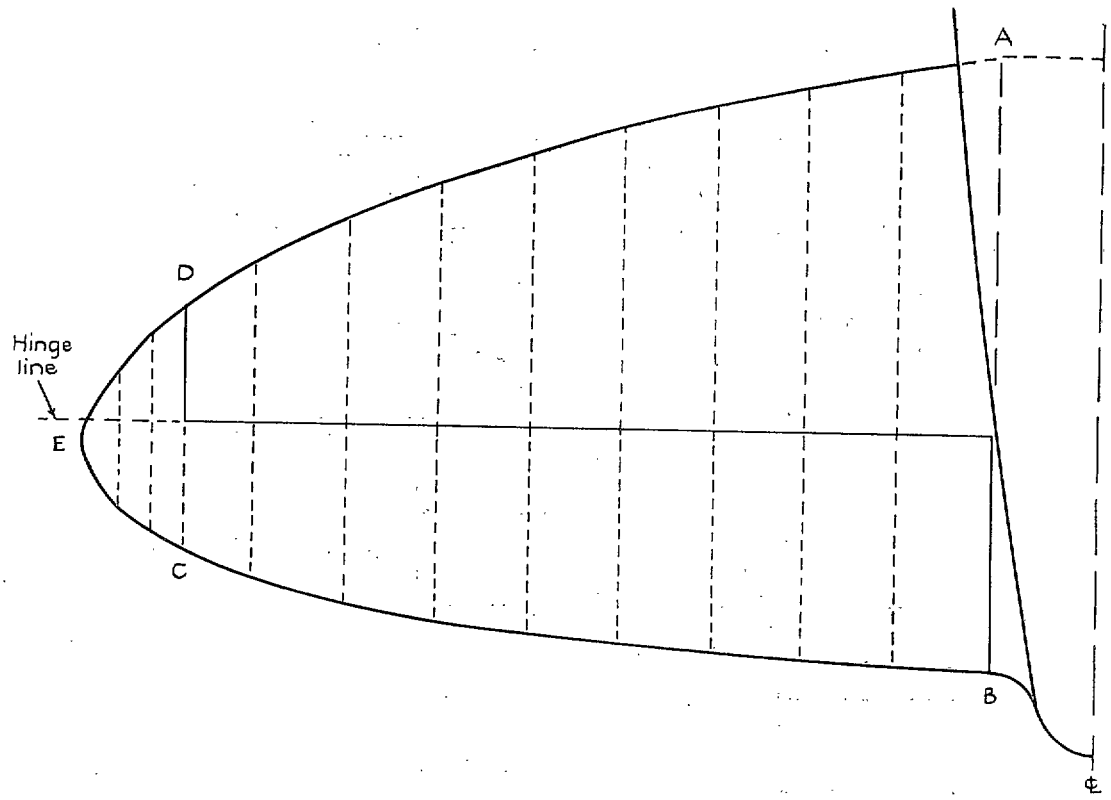

FIG. 7. The strips used in the calculation.

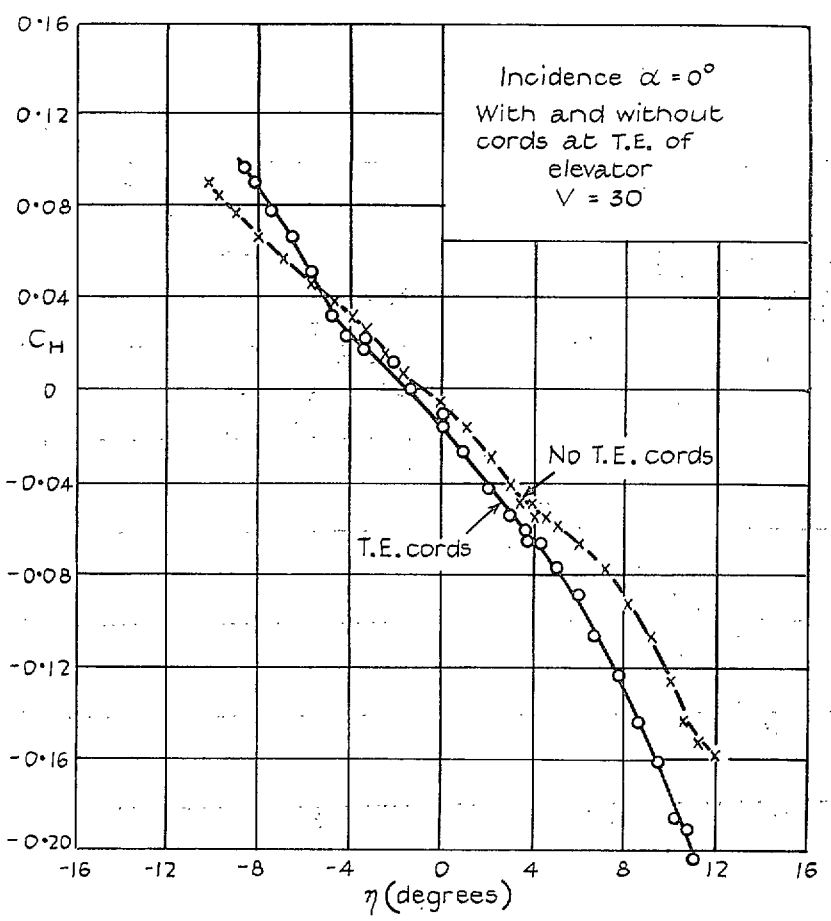

FIG. 8. Variation of static hinge moment with elevator angle.

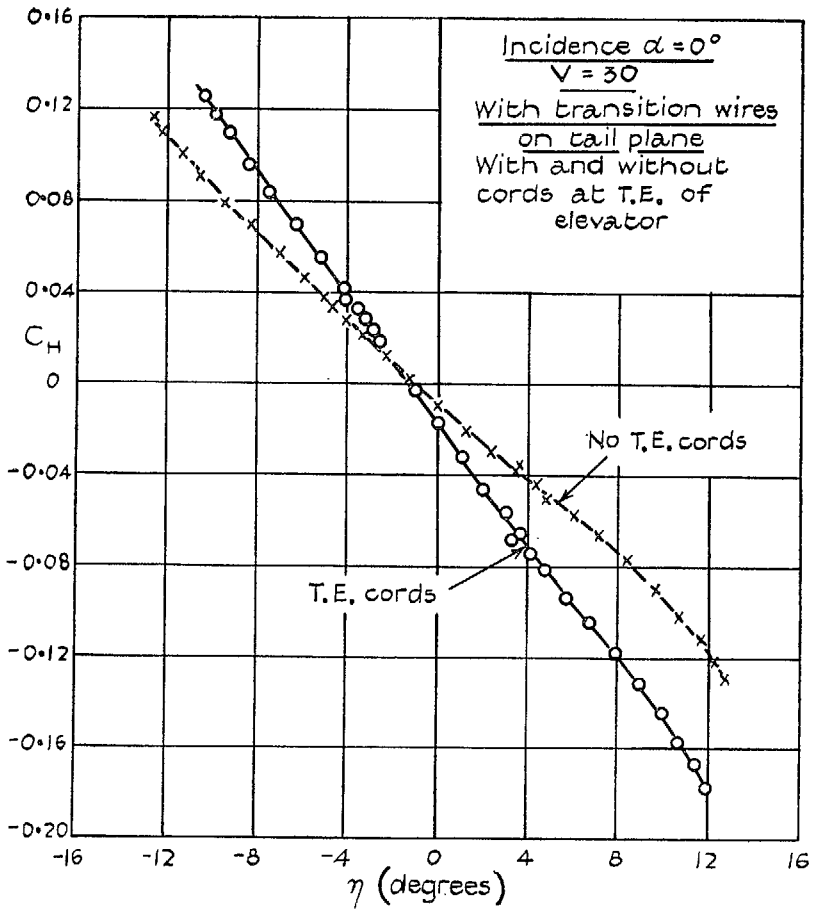

FIG. 9. Variation of static hinge moment with elevator angle.

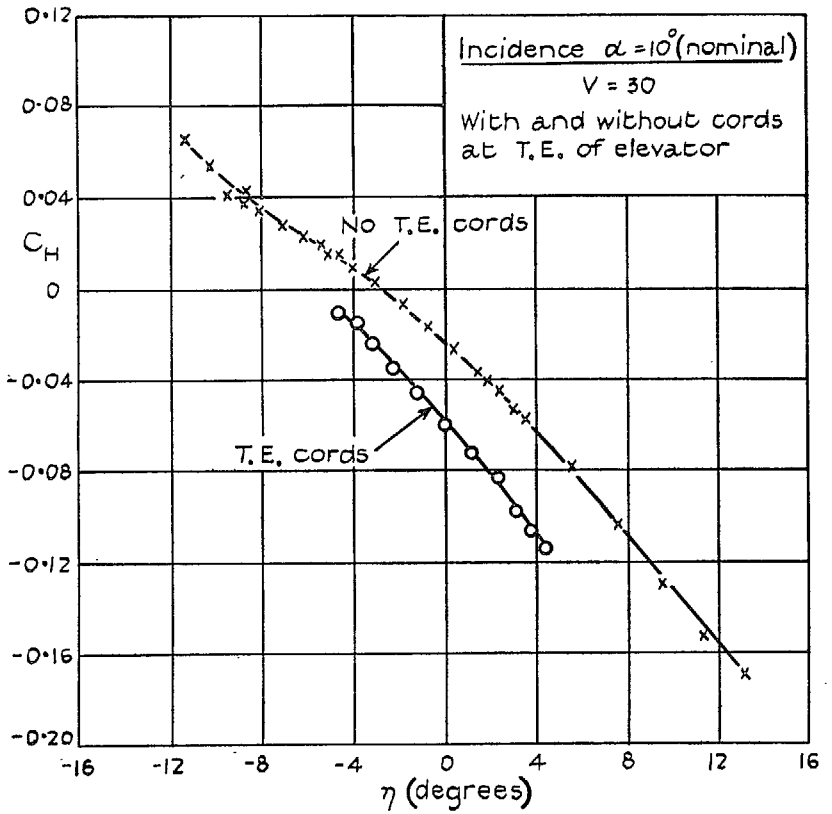

FIG. 10. Variation of static hinge moment with elevator angle.

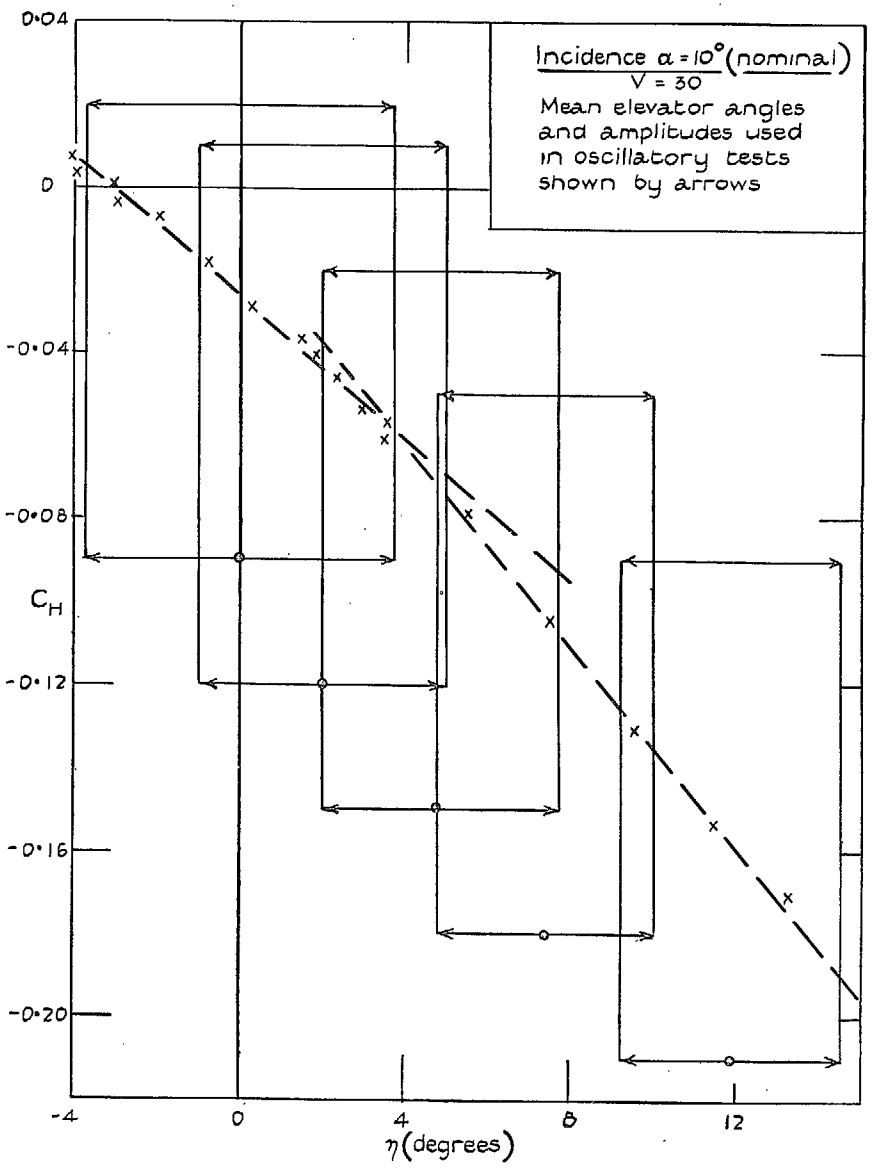

FIG. 11. Variation of static hinge moment with elevator angle, and the ranges used in the oscillatory tests.

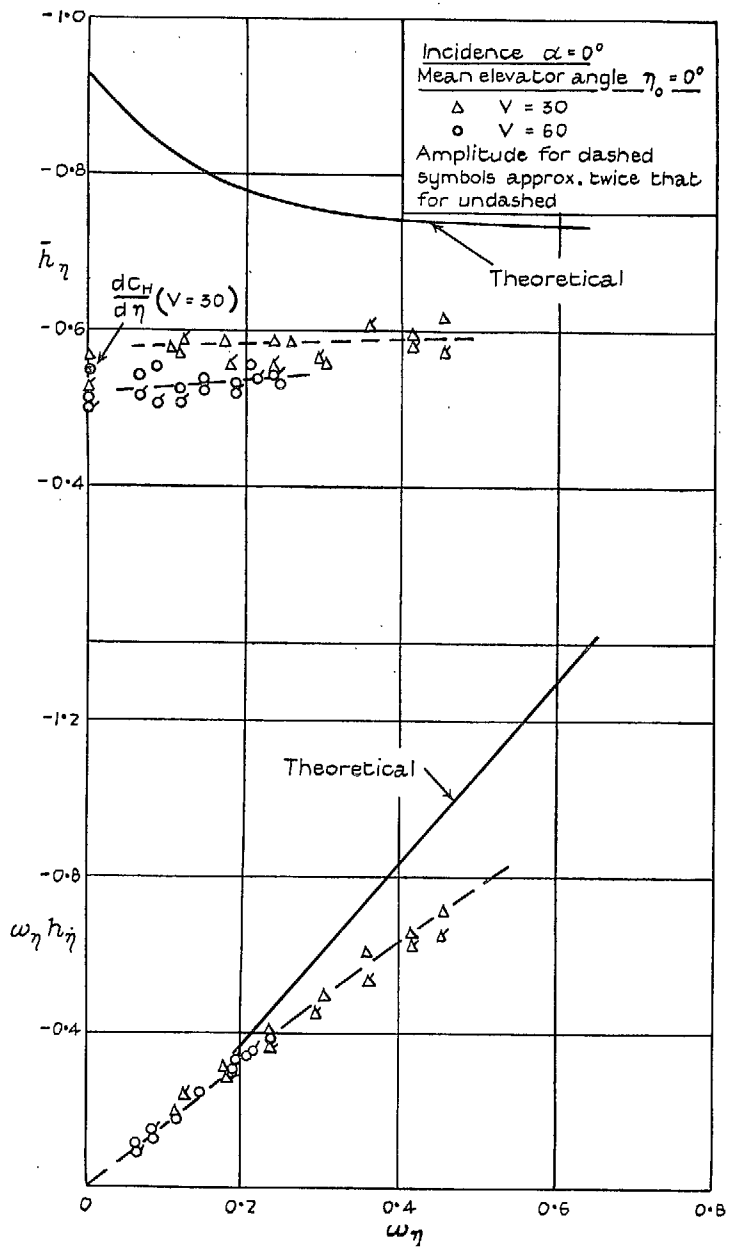

FIG. 12. Variation of stiffness and damping derivative coefficients with frequency parameter.

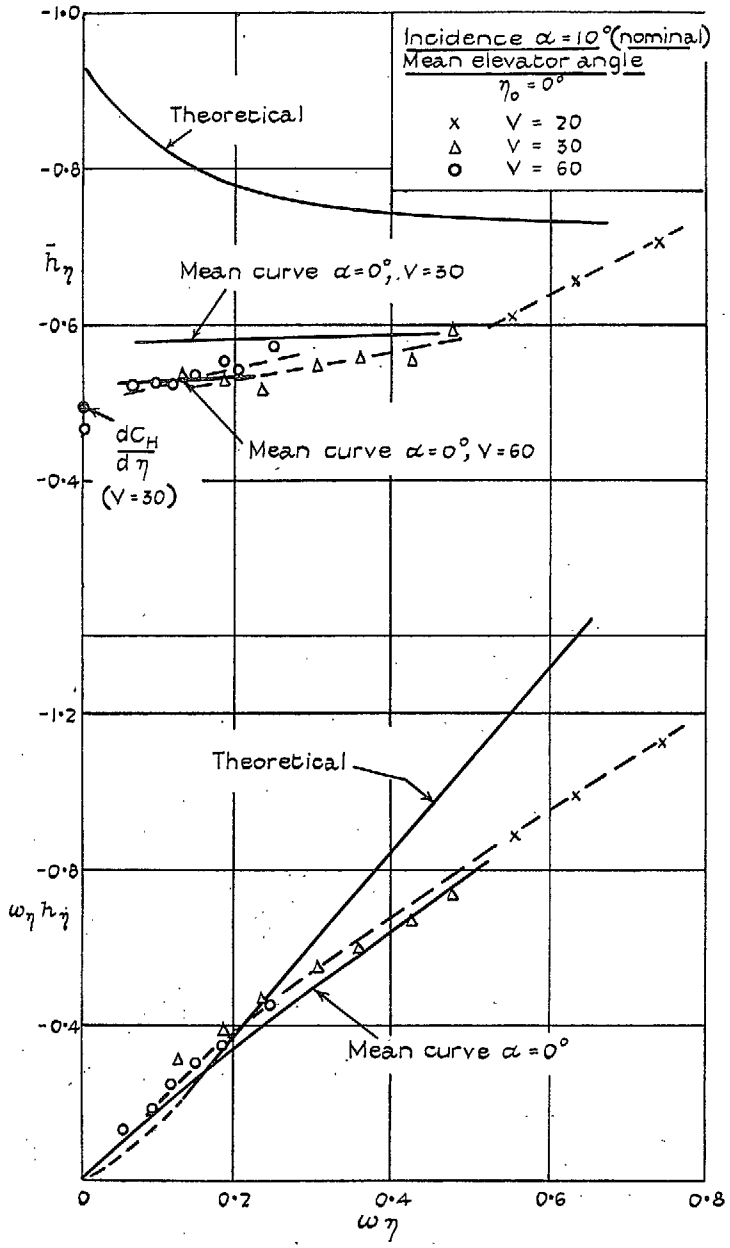

FIG. 13. Variation of stiffness and damping derivative coefficients with frequency parameter.

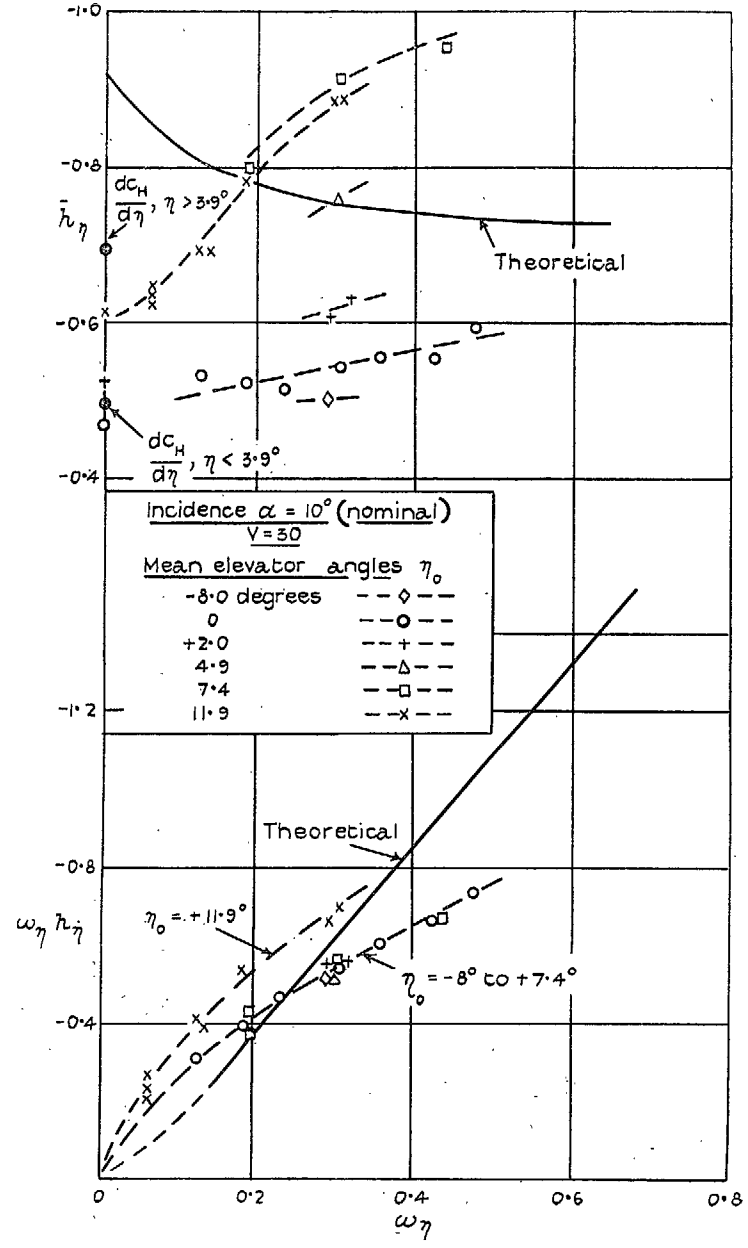

FIG. 14. Variation of stiffness and damping derivative coefficients with frequency parameter.

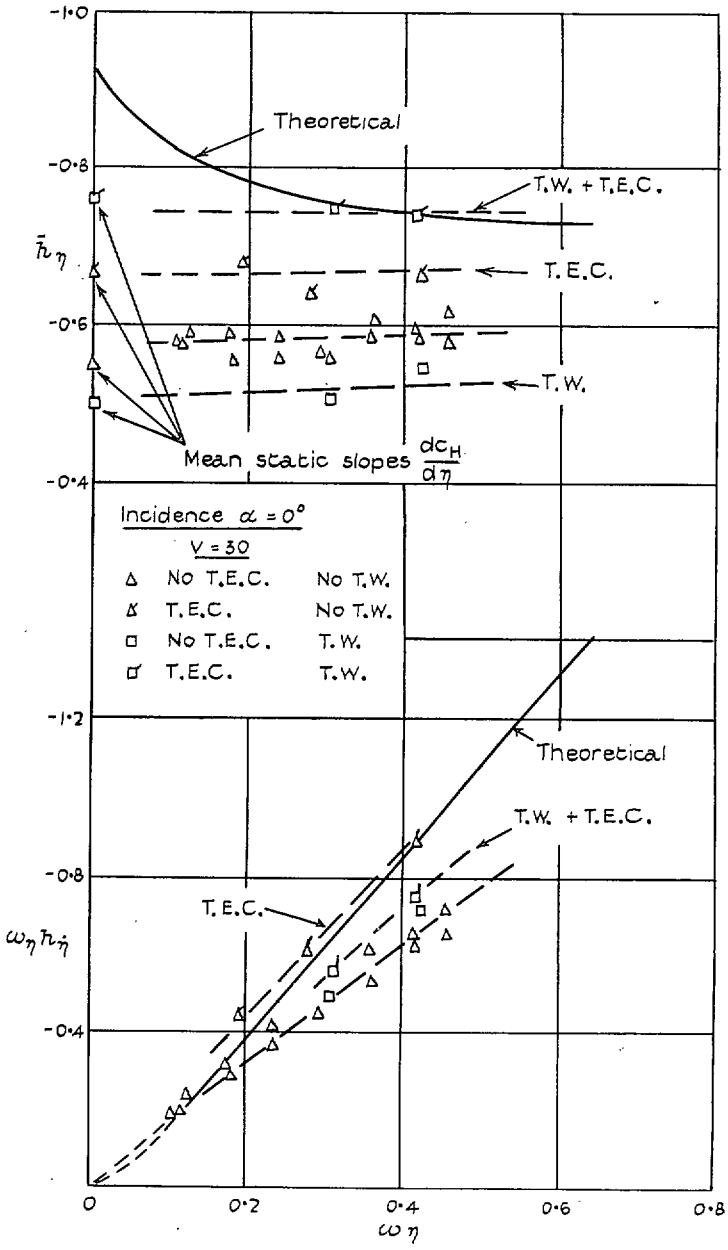

FIG. 15. Variation of stiffness and damping derivative coefficients with frequency parameters. Combinations of trailing-edge cords (T.E.C.) and transition wires (T.W.).

(52307) Wt. 15/680 K.9 7/53 Hw. PRINTED IN GREAT BRITAIN

Publications of the Aeronautical Research Council

ANNUAL TECHNICAL REPORTS OF THE AERONAUTICAL RESEARCH COUNCIL (BOUND VOLUMES)

1936 Vol. I. Aerodynamics General, Performance, Airscrews, Flutter and Spinning. 40*s.* (40*s.* 9*d.*)
Vol. II. Stability and Control, Structures, Seaplanes, Engines, etc. 50*s.* (50*s.* 10*d.*)

1937 Vol. I. Aerodynamics General, Performance, Airscrews, Flutter and Spinning. 40*s.* (40*s.* 10*d.*)
Vol. II. Stability and Control, Structures, Seaplanes, Engines, etc. 60*s.* (61*s.*)

1938 Vol. I. Aerodynamics General, Performance, Airscrews. 50*s.* (51*s.*)
Vol. II. Stability and Control, Flutter, Structures, Seaplanes, Wind Tunnels, Materials. 30*s.* (30*s.* 9*d.*)

1939 Vol. I. Aerodynamics General, Performance, Airscrews, Engines. 50*s.* (50*s.* 11*d.*)
Vol. II. Stability and Control, Flutter and Vibration, Instruments, Structures, Seaplanes, etc. 63*s.* (64*s.* 2*d.*)

1940 Aero and Hydrodynamics, Aerofoils, Airscrews, Engines, Flutter, Icing, Stability and Control, Structures, and a miscellaneous section. 50*s.* (51*s.*)

1941 Aero and Hydrodynamics, Aerofoils, Airscrews, Engines, Flutter, Stability and Control, Structures. 63*s.* (64*s.* 2*d.*)

1942 Vol. I. Aero and Hydrodynamics, Aerofoils, Airscrews, Engines. 75*s.* (76*s.* 3*d.*)
Vol. II. Noise, Parachutes, Stability and Control, Structures, Vibration, Wind Tunnels. 47*s.* 6*d.* (48*s.* 5*d.*)

1943 Vol. I. (*In the press.*)
Vol. II. (*In the press.*)

ANNUAL REPORTS OF THE AERONAUTICAL RESEARCH COUNCIL—

1933–34	1*s.* 6*d.* (1*s.* 8*d.*)	1937	2*s.* (2*s.* 2*d.*)
1934–35	1*s.* 6*d.* (1*s.* 8*d.*)	1938	1*s.* 6*d.* (1*s.* 8*d.*)
April 1, 1935 to Dec. 31, 1936.	4*s.* (4*s.* 4*d.*)	1939–48	3*s.* (3*s.* 2*d.*)

INDEX TO ALL REPORTS AND MEMORANDA PUBLISHED IN THE ANNUAL TECHNICAL REPORTS, AND SEPARATELY—

April, 1950 - - - - R. & M. No. 2600. 2*s.* 6*d.* (2*s.* 7½*d.*)

AUTHOR INDEX TO ALL REPORTS AND MEMORANDA OF THE AERONAUTICAL RESEARCH COUNCIL—

1909–1949. R. & M. No. 2570. 15*s.* (15*s.* 3*d.*)

INDEXES TO THE TECHNICAL REPORTS OF THE AERONAUTICAL RESEARCH COUNCIL—

December 1, 1936 — June 30, 1939.	R. & M. No. 1850.	1*s.* 3*d.* (1*s.* 4½*d.*)
July 1, 1939 — June 30, 1945.	R. & M. No. 1950.	1*s.* (1*s.* 1½*d.*)
July 1, 1945 — June 30, 1946.	R. & M. No. 2050.	1*s.* (1*s.* 1½*d.*)
July 1, 1946 — December 31, 1946.	R. & M. No. 2150.	1*s.* 3*d.* (1*s.* 4½*d.*)
January 1, 1947 — June 30, 1947.	R. & M. No. 2250.	1*s.* 3*d* (1*s.* 4½*d.*)
July, 1951.	R. & M. No. 2350.	1*s.* 9*d.* (1*s.* 10½*d.*)

Prices in brackets include postage.

Obtainable from

HER MAJESTY'S STATIONERY OFFICE

York House, Kingsway, London, W.C.2; 423 Oxford Street, London, W.1 (Post Orders: P.O. Box 569, London, S.E.1); 13a Castle Street, Edinburgh 2; 39, King Street, Manchester, 2; 2 Edmund Street, Birmingham 3; 1 St. Andrew's Crescent, Cardiff; Tower Lane, Bristol 1; 80 Chichester Street, Belfast, or through any bookseller